



HAL
open science

SHM for RC Structure Using PZT Rebar Active Sensing System - Numerical Study

Fan Wu, Wanjun Li, Juan Yi

► **To cite this version:**

Fan Wu, Wanjun Li, Juan Yi. SHM for RC Structure Using PZT Rebar Active Sensing System - Numerical Study. EWSHM - 7th European Workshop on Structural Health Monitoring, IFFSTTAR, Inria, Université de Nantes, Jul 2014, Nantes, France. hal-01020430

HAL Id: hal-01020430

<https://inria.hal.science/hal-01020430>

Submitted on 8 Jul 2014

HAL is a multi-disciplinary open access archive for the deposit and dissemination of scientific research documents, whether they are published or not. The documents may come from teaching and research institutions in France or abroad, or from public or private research centers.

L'archive ouverte pluridisciplinaire **HAL**, est destinée au dépôt et à la diffusion de documents scientifiques de niveau recherche, publiés ou non, émanant des établissements d'enseignement et de recherche français ou étrangers, des laboratoires publics ou privés.

SHM FOR RC STRUCTURE USING PZT REBAR ACTIVE SENSING SYSTEM – NUMERICAL STUDY

Fan Wu¹, Wanjun Li¹, Juan Yi¹

¹*Department of Civil Engineering, School of Naval Architecture, Ocean, and Civil Engineering,
Shanghai Jiao Tong University, Shanghai, China*

fanwu@sjtu.edu.cn

ABSTRACT

An active sensing diagnostic system using PZT for SHM of reinforced concrete structure has been currently under the investigation. The system consists of steel reinforcement bar (rebar) and PZTs bonded on the rebar surface. Test results show that the system can detect damages of the structure. To fundamentally understand the damage algorithm and therefore to establish a robust diagnostic mechanism, an accurate Finite Element Analysis (FEA) for the system has been performed. Reinforced concrete structure with a PZT bonded rebar is also simulated and analyzed with commercial FEA software. Simulation analysis is further made for concrete structure with different debonding damage sizes, and the results are validated with test ones. A series of signal optimization have been done through simulated parametric studies. Improvement of PZT installation has been discussed and the relationship between improvement and signal output has been established. By increasing both sizes of PZT actuators and sensors, the output signals increase linearly with PZT size and by several times.

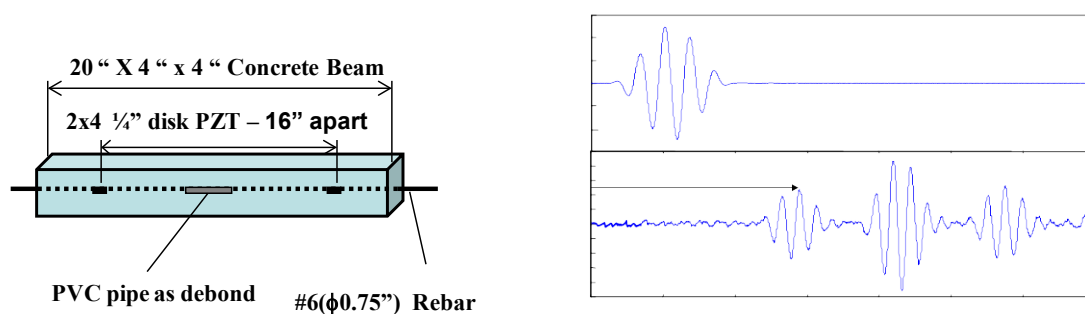
KEYWORDS: *PZT, SHM, RC structure damage detection, numerical study*

1 INTRODUCTION

The guided stress wave method uses time of arrival and amplitude change of signals to detect defects of a structure[1-3]. And the surface guided wave methods have been successfully applied for crack detection in concrete structures [4,5]. In fact, PZT elements are very suitable for integration into the concrete structures as an in-situ actuator/sensor because of the low cost and the properties mentioned above. Recently, an active sensing diagnostic system using PZT for SHM of concrete structures has been under investigation [6].

Experimental tests have been conducted on concrete beam component (20in. x4in. x4in.) with a steel reinforcement bar ($\phi 0.75$ in.) in the middle of each component (Figure 1a). A 90 kHz five-peak burst ultrasonic wave with a peak value of 200V was applied to the actuators. This wave type has been frequently used in structural health evaluations [7-9] because of its sensitivity to the anomalies in the wave propagating medium. The amplitudes and time of arrival of the first wave peak from sensors were recorded and analyzed, and signal changes between the data of baseline and after the damage were evaluated (Figure 1b).

Test results show that the crack /debonding damage in RC structures could be detected using such a PZT based active sensing diagnostic system. The amplitude of the sensor output increases as the extent of crack/debond increases[3]. And it is further found that signal's amplitude is exponentially increased with the damage size.



a) Layout of the PZT rebar concrete beam

b) Test wave and the principle of SHM

Figure 1: PZT based active sensing SHM system for concrete beam

Due to the complexity of concrete microstructure and PZT’s coupling effect of structural and electrical fields, numerical simulation turns to be a good approach for analyzing such an SHM system. A lot of work has been done using numerical simulation for PZT based SHM for different structures[10-12]. Most of the work did not simulate epoxy layer which bonded PZT to the structures, and some even didn’t simulate PZT due to software limitation. Our simulation used 2D axi-symmetrical modeling, which greatly simplifies the modeling complexity and saves the elements needed for 3D. This enabled us to simulate many details set in the tests, including the epoxy layer and voids around PZT.

In this paper, simulation for reinforcement bar bonded with PZT was first carried out and validate with experimental testing results, and then the debonding detection for concrete beam was simulated and validated. Further these models were used to explore the possible signal improvement.

2 NUMERICAL SIMULATION

2.1 Meshing

A partial mesh figure for the FE model of a steel reinforcement bar with PZT is shown in Figure 2. Using 2 dimensional (2D) axi-symmetric modeling, the mesh consisted of 3 layers in vertical for steel rebar, i.e., steel, silver-epoxy and PZT. And the void between steel bar and PZT was also simulated. Similarly, the concrete beam component with a PZT rebar (Figure 1a) was simulated with 2D axi-symmetric model type. Its mesh consisted of 4 layers, with concrete covered on the top of PZT rebar.

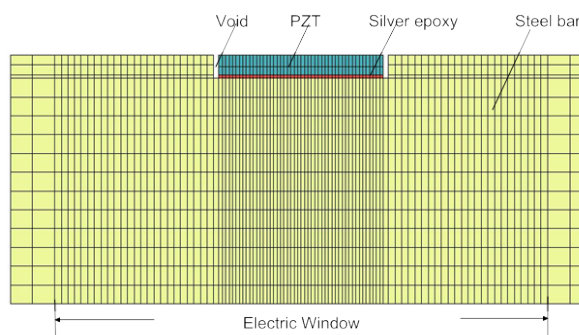


Figure 2: Mesh design of a steel rebar with PZTs (partial)

To get converge to the ideal results, at least 20 elements have to be used for each wavelength along the direction of wave propagation[3,13]. In our model, a finer mesh has been used, and different mesh sizes on and around the PZT were applied for performance purpose – which formed

an electric window effect (Figure 2) [7]. The maximum time step set was less than 1/10 of the central frequency.

2.2 Property Configuration

The configuration of material properties for the FE model includes those for steel rebar, silver epoxy, PZT and concrete. Because of the electrical-mechanical coupling effect of PZT, it has unique properties including the elastic stiffness tensor C , the piezoelectric strain constant tensor d , and the permittivity matrix ε . Notice that for 2D axi-symmetric modeling, the coordinate system defined in ANSYS is different from what in IEEE, which the properties of PZT product are based on. Therefore, coordinate transformation had to be performed before setting up the constants for these tensors and matrix [14]. Further, since the polarization direction in IEEE is in z direction, while in ANSYS it is in x direction for 2D axi-symmetric model, extra step of coordinate transformation was needed for tensor d .

Rayleigh damping was selected in the simulation. The stiffness damping ratio β [15] was set as 3.54×10^{-10} . For steel rebar simulation, extra value had to be used to depress the numerical noise. The β was set as 1.0×10^{-8} . The decrease of output's amplitude due to the noise depression would be compensated back, and the lost value could be found by the relationship between the amplitude and the damping value through numerical simulation.

3 RESULTS

3.1 Validation

3.1.1 Validation for PZT steel rebar

Validation of numerical model for PZT steel rebar has been performed by adding 200V 90KHz 5-peak burst transient waves onto PZT actuators. The analysis used the transient dynamics type which could fully simulate the PZT electrical-mechanical coupling effect. The various material properties are illustrated in Table 1. The distance between sensors and actuators was 16in (406.4mm). The properties for PZT material are based on PZT-850 of APC Corp. of USA.

Table 1. Material Properties using in Simulation

Property constant (unit)	Value
PZT Coefficient d_{33} (m/V)	-175×10^{-12}
PZT Coefficient d_{13} (m/V)	400×10^{-12}
PZT Relative Dielectric Constant $\varepsilon_{11}/\varepsilon_0$	1700
PZT Relative Dielectric Constant $\varepsilon_{33}/\varepsilon_0$	1470
Stiffness Constant for PZT Material C_{11} (N/m ²)	12.6×10^{10}
Stiffness Constant for PZT Material C_{33} (N/m ²)	11.7×10^{10}
Stiffness Constant for PZT Material C_{44} (N/m ²)	2.3×10^{10}
Stiffness Constant for PZT Material C_{12} (N/m ²)	7.95×10^{10}
Stiffness Constant for PZT Material C_{13} (N/m ²)	8.41×10^{10}
Young's Modulus for Steel E_s (N/m ²)	20.6×10^{10}
Material Density for Steel ρ_s (kg/m ³)	7900

Poisson Ratio for Steel ν_s	0.3
Damping Ratio for steel ζ_s	0.003
Young's Modulus for Silver Epoxy E_e (N/m ²)	0.875×10^{10}
Material Density for Silver Epoxy ρ_e (kg/m ³)	2800
Poisson Ratio for Silver Epoxy ν_e	0.3

The simulated result was compared with the test result in Figure 3, and it shows a very good match between these two. This validates that the FEA model for a steel rebar with PZT was quite precise. Further parameter studies for signal improvement could be performed based on the model. Moreover, from the time of arrival of signals, it shows that the wave speed was about 4461m/s, implies that it was longitudinal p-wave who dominated the propagation of waves in the rebar case here.

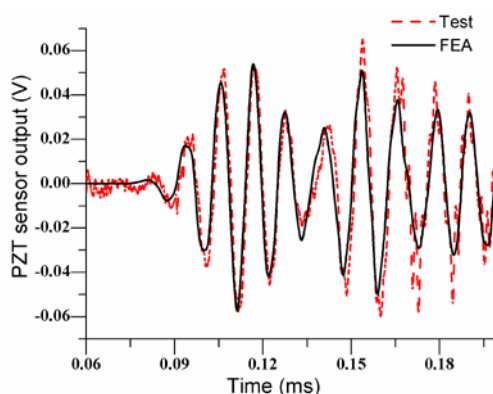


Figure 3: Sensor output from simulation and test for PZT steel rebar

3.1.2 Validation for Concrete Beam Component

Validation of numerical model for concrete beam component with PZT steel rebar has been performed. 2D axi-symmetric model type has been used for the component. Since concrete material is highly inhomogeneous, wave energy dissipates greatly during wave propagation. To simplify the model, concrete was simulated as homogeneous material, but a high damping ratio with 100 dB has been applied. The debonding sizes of 1 inch, 2 inch, 4 inch, and 8 inch have been simulated respectively. Besides of the material properties mentioned in Table 1, the concrete properties were set as follows: the density $\rho_c=2400\text{kg/m}^3$, Young's modulus $E_c=2.8 \times 10^{10}\text{N/m}^2$, and Poisson ratio $\nu_c=0.2$. Because of the large damping effect of concrete, numerical noise was not appeared, and the damping ratio for steel bar did not need to be adjusted, i.e., damping ratio used was 3.54×10^{-10} .

Numerical results for different debonding sizes are shown in Figure 4. By comparisons, the corresponding test results are shown in the same charts. It could be seen that these two sets of results match well, which validates the numerical model. The speed of wave propagation on the rebar was around 3500 m/s. And the dispersion of waves could be observed from all of the charts. Dispersion was attributed to concrete surrounding the bar, which served as an elastic foundation to the bar. As the debonding size increased, the interference of waves from the concrete to the bar surface became less important, resulting in more energy propagating into the bar, which corresponded to larger signal amplitude and less wave dispersion in the results.

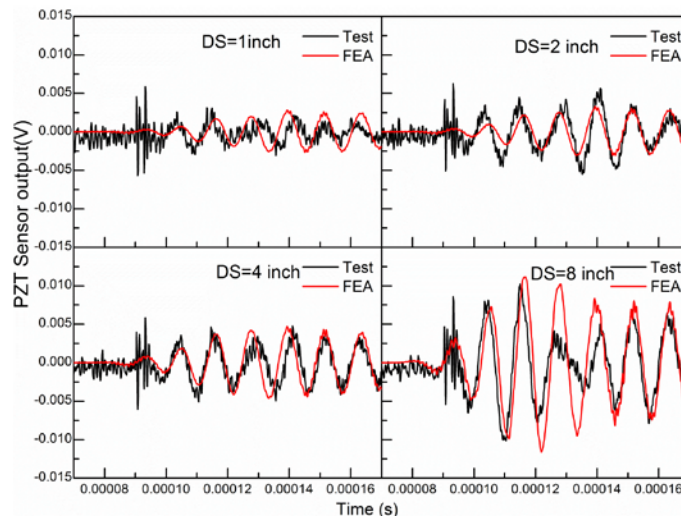


Figure 4: Sensor output from simulation and test for beam with debonding damage

3.2 System Optimization

From above validations, it could be noticed that the output from PZT sensors were very small, comparing to the input of 200V. How to improve the strength of the signals becomes critical for this PZT based active sensing diagnostic system. Optimization has been performed in two parts, i.e., improvement of PZT installation and the PZT size, based on the above numerical analysis.

3.2.1 Optimization of PZT installation

By analyzing the forces in the simulated models, we've found that the waves arriving to PZT were carried out by shear stresses acting on the bottom of PZT surface, i.e., shear stresses were transferred from rebar to epoxy layer then to the PZT. Based on that, one improvement suggested was to fill in the voids between PZT and rebar with solid materials. By filling voids with silver epoxy, the output signals from sensors increased almost 6 times (Figure 5). Further by analyzing the forces acting on the PZT, it was found that both normal stresses on the side of PZT thickness and shear stresses at the PZT bottom had significant values, which proved that both type of forces contributed to the conversion of sensor output voltages.

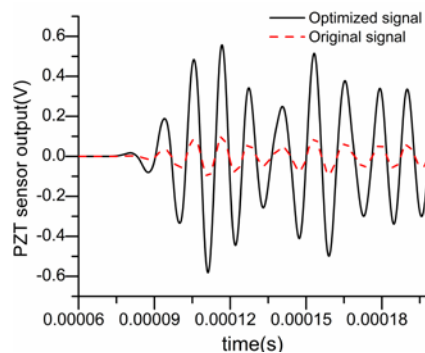


Figure 5: Sensor output of optimization of void width filled with silver epoxy

Further parametric study for the void width filled with silver epoxy has been performed. Notice that the void width in above optimization (Figure 5) was set as 0.2mm, and corresponding output was about 0.56V. Parametric study shows that the relationship between width and the amplitude of

output could be mapped with a decrease exponential curve (Figure 6), i.e., the output increased exponentially as the width decreased. And the signal increase was about 1.5 times from width of 0.6mm to 0.2mm.

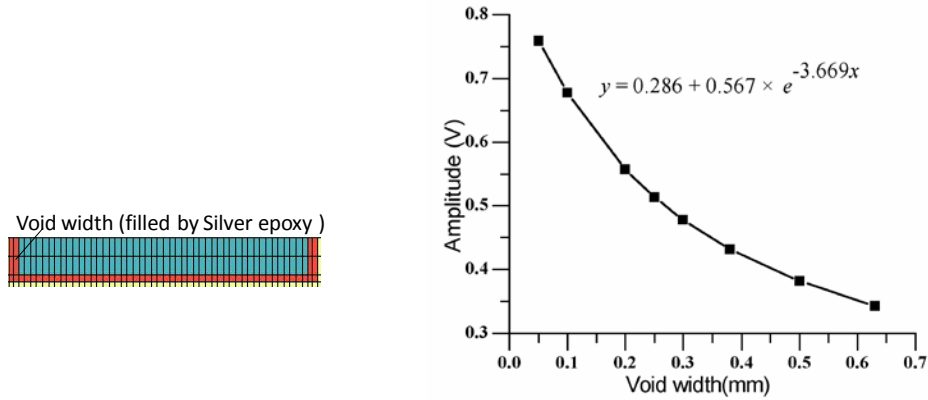
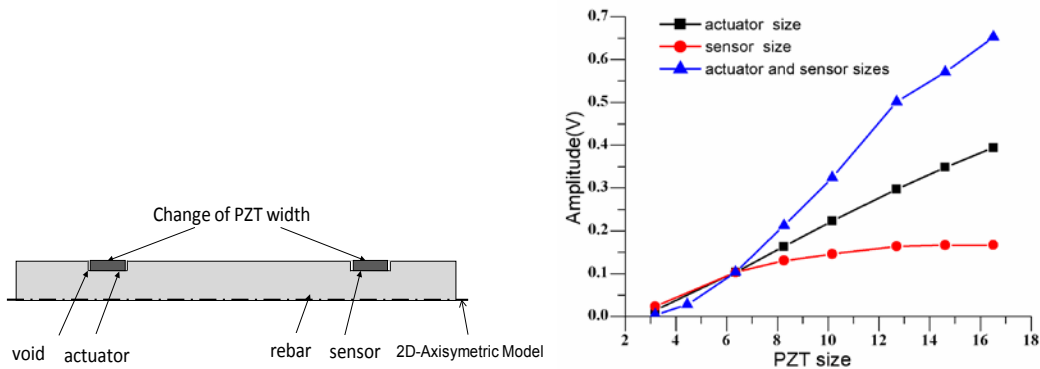


Figure 6: Parametric study of void width filled with silver epoxy

3.2.2 Optimization of PZT sizes

Parametric studies for PZT sizes have been done for signal optimization purpose. By keeping PZT's thickness the same, the width of PZT for both actuators and sensors have been changed, and different combinations of changes have been simulated. During optimization, the voids between PZT and rebar on actuators and sensors were not filled (Figure 7a).

It could be observed from Figure 7b that the changes of sensor-size-only would lead to increase of the output, but the effect was limited. It would be saturated to a limit as the sensor size increased to a certain value. However, the change of actuator-size-only would lead to the linear increase of sensor output. And changes of both actuator and sensor sizes would lead to faster linear increase of sensor output. Figure 7b provides the details of the output changes with PZT sizes. The output increased almost 3 times by doubling the size of actuator, and it further increased almost 5 times by doubling both actuator and sensor sizes.



a) Layout of PZT size optimization b) Sensor output changes with different PZT sizes

Figure 7: Signal optimization with PZT sizes

4 CONCLUSIONS

Numerical simulation with detailed 2D axi-symmetric modeling for a PZT active sensing system for damage detection of concrete structure has been demonstrated here. Validations show that

numerical results match well with test results. System optimization has been done by changing both PZT installation and PZT size. It suggests that such optimization could improve system output with magnitudes. Future work will be concentrated on performing experimental tests by applying the optimization onto the specimens. And detection for other damage types such as crack will be investigated through the simulation. Numerical simulation using 3D model for the active sensing system and the concrete structure is under investigation.

ACKNOWLEDGEMENT

The authors gratefully acknowledge the financial supports provided by National Science Foundation of China under grants No. NSFC-51278300 and No. NSFC-61227071.

REFERENCES

- [1] S. Ha and F. K. Chang, "Optimizing a spectral element for modeling PZT-induced Lamb wave propagation in thin plates," *Smart Materials and Structures*, Papers 19, 1-11 (2010).
- [2] F. Song, G. L. Huang, J. Kim, and S. Haran, "On the study of surface wave propagation in concrete structures using a piezoelectric actuator/sensor system," *Smart Materials and Structures*, Papers 17, 1-8(2008).
- [3] F. Wu and F. K. Chang, "Debond detection using embedded piezoelectric elements for reinforced concrete structures-Part II: Analysis and algorithm," *Structural Health Monitoring*, Papers 5, 17-28(2006).
- [4] J. S. Popovics, W. J. Song, M. Ghandehari, K. V. Subramaniam, J. D. Achenbach, and S. P. Shah, "Application of Surface Wave Transmission Measurements for Crack Depth Determination in Concrete," *Materials Journal*, Papers 97, 127-135(2000).
- [5] S. W. Shin, C. B. Yun, J. S. Popovics, and J. H. Kim, "Improved Rayleigh Wave Velocity Measurement for Nondestructive Early-Age Concrete Monitoring," *Research in Nondestructive Evaluation*, Papers 18, 45-68(2007).
- [6] F. Wu and F. K. Chang, "Debond detection using embedded piezoelectric elements in reinforced concrete structures-part I: experiment," *Structural Health Monitoring*, Papers 5, 5-15(2006).
- [7] J. M. Berthelot, S. M. Ben, and J. L. Robert, "Study of wave attenuation in concrete," *Journal of Materials Research*, Papers 8, 2344-2353(1993).
- [8] L. Bond, "Methods for the Computer Modeling of Ultrasonic Waves in Solids." *Research Techniques in Nondestructive Testing*, Papers 6, 107-150(1982).
- [9] E. F. Crawley and E. H. Anderson, "Detailed Models of Piezoceramic Actuation of Beams," *Journal of Intelligent Material Systems and Structures*, Papers 1, 14-25(1990).
- [10] S. Park, S. Ahmad, C. B. Yun, and Y. Roh, "Multiple crack detection of concrete structures using impedance-based structural health monitoring techniques," *Experimental Mechanics*, Papers 46, 609-618(2006).
- [11] A. Raghavan and C. E. S. Cesnik, "Finite-dimensional piezoelectric transducer modeling for guided wave based structural health monitoring," *Smart Materials and Structures*, Papers 14, 1448-1461(2005).
- [12] K. K. Tseng and L. Wang, "Smart piezoelectric transducers for in situ health monitoring of concrete," *Smart Materials and Structures*, Papers 13, 1017-1024(2004).
- [13] K. J. Bathe, [Finite Element Procedures], *Englewood Cliffs: Upper Saddle River*, New Jersey, (1996).
- [14] S. Moharana and S. Bhalla, "Numerical investigations of shear lag effect on PZT-structure interaction: review and application," *Current Science*, Papers 103, 685-696(2012).
- [15] L. Cremer and M. Heckl, [Structure-Borne Sound], *Springer*, (1988).